Argonne NATIONAL LABORATORY

ANL/DIS-13/06

Modeling Adjustable Speed Pumped Storage Hydro Units Employing Doubly-Fed Induction Machines

Decision and Information Sciences

About Argonne National Laboratory

Argonne is a U.S. Department of Energy laboratory managed by UChicago Argonne, LLC under contract DE-AC02-06CH11357. The Laboratory's main facility is outside Chicago, at 9700 South Cass Avenue, Argonne, Illinois 60439. For information about Argonne and its pioneering science and technology programs, see www.anl.gov.

Availability of This Report

This report is available, at no cost, at http://www.osti.gov/bridge. It is also available on paper to the U.S. Department of Energy and its contractors, for a processing fee, from:

U.S. Department of Energy
Office of Scientific and Technical Information
P.O. Box 62
Oak Ridge, TN 37831-0062
phone (865) 576-8401
fax (865) 576-5728
reports@adonis.osti.gov

ANL/DIS-13/06

Modeling Adjustable Speed Pumped Storage Hydro Units Employing Doubly-Fed Induction Machines

prepared for
U.S. Department of Energy – Wind and Water Power Technologies Office

prepared by
Vladimir Koritarov and Leah Guzowski
Decision and Information Sciences, Argonne National Laboratory

James Feltes, Yuriy Kazachkov and Bo Gong
Siemens PTI

Bruno Trouille and Peter Donalek
MWH Americas

August 2013

This page intentionally left blank.

Preface

This report is one of several reports developed during the U.S. Department of Energy (DOE) study on the Modeling and Analysis of Value of Advanced Pumped Storage Hydropower in the United States. The study is led by Argonne National Laboratory in collaboration with Siemens PTI, Energy Exemplar, MWH Americas, and the National Renewable Energy Laboratory. Funding for the study was provided by DOE's Office of Energy Efficiency and Renewable Energy (EERE) through a program managed by the EERE's Wind and Water Power Technologies Office (WWPTO).

The scope of work for the study has two main components: (1) development of vendor-neutral dynamic simulation models for advanced pumped storage hydro (PSH) technologies, and (2) production cost and revenue analyses to assess the value of PSH in the power system. Throughout the study, the project team was supported and guided by an Advisory Working Group (AWG) consisting of more than 30 experts from a diverse group of organizations, including the hydropower industry and equipment manufacturers, electric power utilities and regional electricity market operators, hydro engineering and consulting companies, national laboratories, universities and research institutions, hydropower industry associations, and government and regulatory agencies.

The development of vendor-neutral models was carried out by the Advanced Technology Modeling Task Force Group (TFG) led by experts from Siemens PTI with the participation of experts from other project team members. First, the Advanced Technology Modeling TFG reviewed and prepared a summary of the existing dynamic models of hydro and PSH plants that are currently in use in the United States. This is published in the report *Review of Existing Hydroelectric Turbine-Governor Simulation Models*. The review served to determine the need for improvements of existing models and for the development of new ones.

While it was found that existing dynamic models for conventional hydro and PSH plants allow for accurate representation and modeling of these technologies, it was concluded that there is a need for the development of dynamic models for two PSH technologies for which at present there are no existing models available in the United States. Those two technologies are (1) adjustable speed PSH plants employing doubly-fed induction machines (DFIMs) and (2) ternary PSH units. The Advanced Technology Modeling TFG developed vendor-neutral models of these two PSH technologies, which are published in two reports: (1) *Modeling Adjustable Speed Pumped Storage Hydro Units Employing Doubly-Fed Induction Machines* and (2) *Modeling Ternary Pumped Storage Units.*

Extensive testing of newly developed models was performed using the Siemens PTI's standard test cases for the Power System Simulator for Engineering (PSS®E) model as well as the Western Electricity Coordinating Council's (WECC's) modeling cases for the Western Interconnection that were provided in PSS®E format. The results of model

testing are presented in the report *Testing Dynamic Simulation Models for Different Types of Advanced Pumped Storage Hydro Units*.

In addition to the project team members and DOE, all these reports have been reviewed by members of the AWG, and their comments and suggestions have been incorporated into the final versions of the reports. Parts of these reports will also be included in the final report for the entire study to illustrate the model development component of the work.

Acknowledgments

The authors would like to acknowledge the support and guidance provided to the project team by the staff and contractors of the U.S. Department of Energy Office of Energy Efficiency and Renewable Energy's (DOE/EERE's) Wind and Water Power Technologies Office (WWPTO), including Michael Reed, Rajesh Dham, Charlton Clark, Rob Hovsapian, Patrick O'Connor, Richard Gilker, and others. The authors are also grateful to the members of the Advisory Working Group for their excellent collaboration and efforts in advising the project team and guiding the study. The Advisory Working Group included a broad spectrum of global pumped storage hydropower specialists.

Rajesh Dham, Charlton Clark, Rob Hovsapian, Patrick O'Connor, Richard Gilker	DOE/EERE – Wind and Water Power Technologies Office (WWPTO)
Rachna Handa	DOE – Office of Electricity Delivery and Energy Reliability (OE)
Rahim Amerkhail	Federal Energy Regulatory Commission (FERC)
Michael Manwaring, Douglas Divine	National Hydropower Association (NHA)
Mark Jones, Elliot Mainzer	Bonneville Power Administration (BPA)
Xiaobo Wang	California Independent System Operator (CAISO)
Zheng Zhou	Midwest Independent System Operator (MISO)
Matt Hunsaker	Western Electricity Coordinating Council (WECC)
Tuan Bui	California Department of Water Resources (CDWR)
David Harpman	Bureau of Reclamation (Reclamation)
Kyle L. Jones	U.S. Army Corps of Engineers (USACE)
Scott Flake, Greg Brownell	Sacramento Municipal Utility District (SMUD)
Paul Jacobson, Stan Rosinski	Electric Power Research Institute (EPRI)
Alan Soneda	Pacific Gas and Electric Co. (PG&E)
Osamu Nagura	Hitachi Mitsubishi Hydro
Teruyuki Ishizuki	Toshiba Corp.
Rick Miller. Rick Jones	HDR Engineering Inc. (HDR|DTA)
Jiri Koutnik, Maximilian Manderla	Voith Hydro
Christophe Nicolet	Power Vision Engineering (PVE)
Peter McLaren	Center for Advanced Power Systems (CAPS)
Landis Kannberg	Pacific Northwest National Laboratory (PNNL)
Klaus Engels	E.ON Wasserkraft GmbH
Kim Johnson	Riverbank Power
Steve Aubert, Le Tang	ABB Switzerland Ltd
Ali Nourai	DNV KEMA

This page intentionally left blank.

Contents

This page intentionally left blank.

Section
1

Introduction

This report is a part of a series of documents to be issued in the course of a U.S. Department of Energy (DOE) project titled “Modeling and Analysis of Value of Advanced Pumped Storage Hydropower in the U.S.” The purpose of this report is to propose a model structure for an adjustable speed pumped storage hydro (PSH) unit employing a doubly-fed induction machine (DFIM).

The use of a DFIM with its rotor windings controlled by a power converter is the present state-of-the-art design for adjustable speed hydro pumped storage units. Although the theoretical basis for the analysis of DFIMs was developed at least 70 years ago (a paper by Charles Concordia et al. in 1942 describes the mathematical modeling and dynamic response of DFIM and refers to even earlier publications), it seems appropriate to provide the fundamental equations governing their dynamic behavior so that the following discussions on modeling these devices for stability studies are more meaningful.

Fortunately, very significant efforts have been previously applied to determine the proper level of modeling required for DFIMs, albeit not specifically for pumped storage units. Previous efforts to describe the theoretical and modeling aspects of DFIMs were related to the development of models for wind turbines employing doubly-fed induction generators. For a period of more than 10 years starting from the early 2000s, a significant evolution has been observed in the approach to modeling this type of electrical machine. While the machines for pumped storage units will be much larger than those used in wind units, and thus the higher currents and voltages may require different power electronic devices, the control strategies and overall responses will be similar.

Section 2 of this report includes a comprehensive review of the basics of the operation of a DFIM, including the theory of this operation for dynamics and steady state.

Section 3 of the report provides a discussion on modeling units employing a DFIM for dynamic stability studies. This discussion takes into account the experience gained in the course of developing Power System Simulator for Engineering (PSS®E) dynamic simulation models of wind units.

Section 4 provides a discussion on modeling of adjustable speed hydro pumped storage power units employing a DFIM. While the focus of this report is on how to model these units in the PSS®E program, the information is provided in a manner that is also applicable to modeling such devices in other commercial power system stability simulation programs.

Section 5 provides a bibliography.

Section
2

Theory of the Dynamic Simulation Model of the Doubly-Fed (Wound Rotor) Induction Machine

The basics of DFIM operation are as follows. As shown in Figure 2-1, the rotor of the machine is connected to the terminals of the machine through a power converter. Therefore, the power converter can control the voltage, current, and frequency in the rotor circuit.

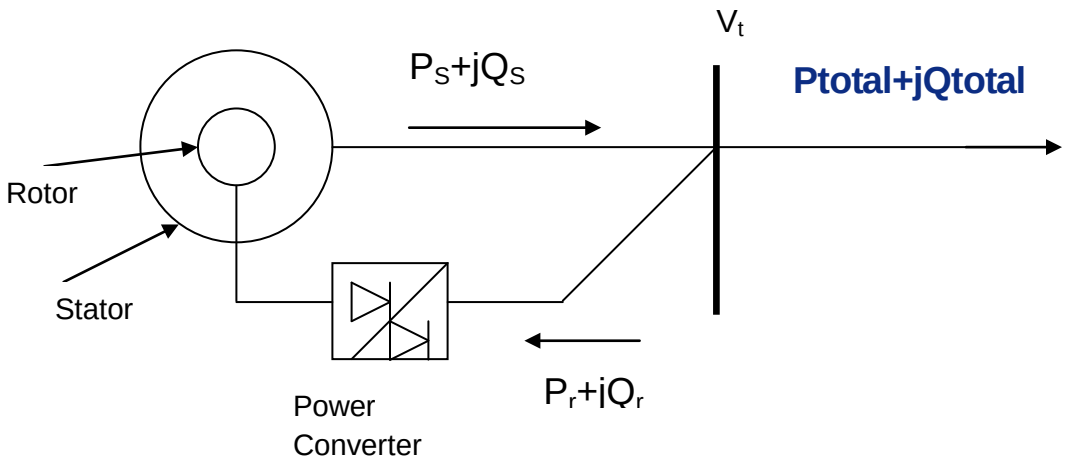

Figure 2-1 Configuration of a DFIM

Neglecting losses:

$$P_r = sP_s,$$

where P_s is the power on the stator in W, P_r is the power on the rotor in W, and s is the slip defined as

$$s = (\omega_1 - \omega_m)/ \omega_1,$$

where ω_1 is the supply angular frequency in electrical rad/s, and ω_m is the rotor mechanical angular frequency in electrical redians per second.

If the generator runs below the synchronous speed ($s > 0$), then $P_r > 0$, and the mechanical power is less than the power on the stator, $P_{mech} < P_s$. The rotor absorbs power, and a fraction of the stator power is absorbed by the rotor circuits.

If the generator runs above the synchronous speed ($s < 0$), then $P_r < 0$ and $P_{mech} > P_s$. The rotor generates power, and power is delivered to the grid via the stator and rotor circuits.

Modern DFIMs employ voltage source power converters utilizing fully controlled transistors. The rotor side converter can supply d and q components of rotor current that determine both active and reactive power at the unit's terminals. The line side converter cannot only transfer the active power from or to the rotor side converter, but also could control the reactive power injected or absorbed by the line side converter to or from the grid. The cycloconverters utilized by the previous generation of variable speed pump storage units did not have this capability. However, for the known applications, the line side power converter usually operates with a unity power factor, that is, the reactive power $Q_r = 0$ Vars.

In a wound rotor induction machine, rotor windings, similar to those of the distributed windings on the stator, are wound on a cylindrical laminated core with uniformly spaced slots on the outer periphery. The terminals of the rotor windings are brought out via slip rings and brushes. The alternating current (AC) terminals of the power converter are connected to the rotor windings via these slip rings to provide slip control.

Figure 2-2 shows the connections and current conventions of the subject machine.

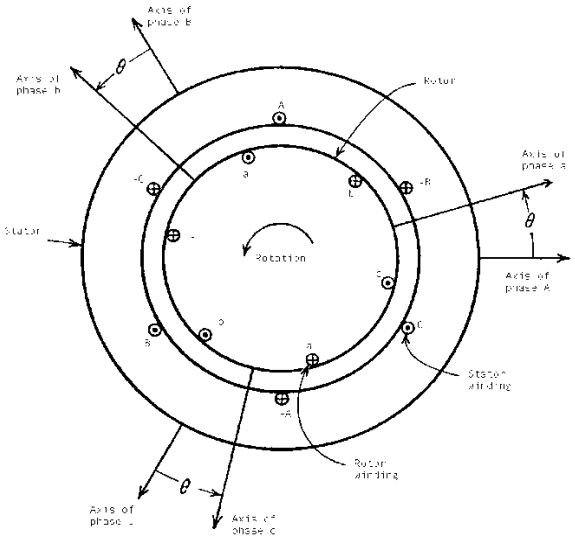

Idealized 3-phase induction machine.

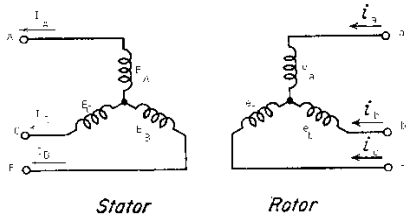

Connections and current conventions for 3-phase induction machine.

Figure 2-2 Connections and Current Conventions Used for the DFIM

In this discussion, capital E, I, and Ψ will be used for stator terminal voltage, current, and flux linkages, respectively. Lower case e, i, and λ are used for rotor terminal voltage, current, and flux linkages, respectively. Capital R and I subscripts indicate components in the real and imaginary axes of the synchronous reference frame, with the imaginary axis I leading the real axis R by 90 electrical degrees.

The following equations are used to describe the dynamic performance of the wound rotor single cage induction machine using the motor convention.

The stator voltage equations are:

$$E_R = \frac{d\Psi_R}{dt} - r_a I_R - \omega_b \Psi_I \qquad (D-1)$$

$$E_I = \frac{d\Psi_I}{dt} - r_a I_I + \omega_b \Psi_R \qquad (D-2)$$

Here ω_b is the base angular frequency in p.u., normalized with respect to synchronous speed. It is introduced for generality. For most studies, ω_b =1.

The rotor voltage equations are:

$$e_R = \frac{d\lambda_R}{dt} + r_1 i_R + (\omega_m - \omega_b)\lambda_I \qquad (D-3)$$

$$e_I = \frac{d\lambda_I}{dt} + r_1 i_I - (\omega_m - \omega_b)\lambda_R \qquad (D-4)$$

Here ω_m is the rotor mechanical angular speed in p.u., normalized with respect to synchronous speed.

Note that both components of the rotor voltage are constant in steady state, similar to the way the R and I components of the synchronous machine stator voltage are constant in steady state.

To be certain of this, one may use the routine conversion formula from the three-phase voltage system to the real and imaginary components with respect to the synchronously rotating reference frame, namely:

$$e_R = \frac{2}{3}[e_A \cos(\delta) + e_B \cos(\delta - 120) + e_C \cos(\delta + 120)]$$

$$e_I = \frac{2}{3}[e_A \sin(\delta) + e_B \sin(\delta - 120) + e_C \sin(\delta + 120)]$$

Here,

- $e_{A,B,C}$ are rotor physical phase voltages which in steady state are of $s\omega$ frequency where s is the rotor mechanical slip, that is,

  $$e_A = E\cos(s\omega t)$$
  $$e_B = E\cos(s\omega t - 120)$$
  $$e_C = E\cos(s\omega t + 120)$$

- δ is the angle between the rotor and the synchronously rotating reference frame, that is,

  $\delta = s\omega t$ electrical degrees

In the course of the dynamic simulation, e_R and e_I are subject to control. Because of this, it is important to realize that changing e_R and e_I actually means changing the magnitude and frequency of the physical rotor phase voltages.

The real and imaginary components of the flux linkages, as functions of stator and rotor currents do not interact; thus they can be written without indices as:

Stator Flux Linkage :

$$\Psi = -L_a I + \Psi_m \qquad (D-5)$$

Mutual Flux Linkage :

$$\Psi_m = L_m(i - I) \qquad (D-6)$$

Wound Rotor Flux Linkage :

$$\lambda = L_1 i + \Psi_m \qquad (D-7)$$

From the equations above, the rotor currents can be expressed as a function of the stator current and rotor flux linkage:

$$i = \frac{\lambda + L_m I}{L_m + L_1} \qquad (D-8)$$

and the stator flux linkages can then be expressed as:

$$\Psi = \frac{L_m}{L_m + L_1}\lambda - I\left(L_a + \frac{L_m L_1}{L_m + L_1}\right) \qquad (D-9).$$

The last equation can be rewritten in a form similar to that used in classical synchronous machine theory by introducing the transient flux linkages:

$$\lambda' = \lambda \frac{L_m}{L_m + L_1} \qquad (D-10)$$

and transient (derived) inductance:

$$L' = L_a + \frac{1}{\frac{1}{L_m} + \frac{1}{L_1}} \qquad (D-11)$$

Then

$$\Psi = \lambda' - IL' \qquad (D-12)$$

The rotor voltage equations (D-3 and D-4) can be rewritten in state space form:

$$\frac{d\lambda_R}{dt} = e_R - r_1 i_R - \lambda_I \, p\theta \qquad (D-13)$$

$$\frac{d\lambda_I}{dt} = e_I - r_1 i_I + \lambda_R \, p\theta \qquad (D-14)$$

where $p\theta = \omega_m - \omega_b$ is a rotor negative slip with respect to the synchronous reference.

Substituting rotor currents from (Equation D-8) into (Equations D-13 and D-14), the rotor transient flux linkages component time derivatives can be found as follows:

$$\frac{d\lambda_R{}'}{dt} = \frac{2\pi f_b}{\omega_b T_0{}'}\left(\frac{L_m}{r_1} e_R - \lambda_R{}' - (L - L')I_R - \omega_b T_0{}' \lambda_I{}' * p\theta\right) \qquad (D-15)$$

$$\frac{d\lambda_I{}'}{dt} = \frac{2\pi f_b}{\omega_b T_0{}'}\left(\frac{L_m}{r_1} e_I - \lambda_I{}' - (L - L')I_I + \omega_b T_0{}' \lambda_R{}' * p\theta\right) \qquad (D-16)$$

where

$$T_0{}' = \frac{L}{\omega_b r_1}$$

$$L = L_1 + L_m$$

The approach to saturation representation is similar to that used in synchronous machines; that is, employing the open circuit saturation curve and entering a flux level that is internal to the machine and empirically approximated as the flux behind transient inductance. The convenience of the transient flux level approach is that, with the use of explicit integration, saturation effects can be represented without requiring iteration of the model equations with the network power flow solutions.

R and I components of the saturation factor will be calculated in proportion to the respective components of the rotor flux linkage.

The differential equations above should be supplemented by equations describing the inertial dynamics.

Electrical torque:

$$T_{el} = -\lambda_I{}' I_R + \lambda_R{}' I_I$$

Rotor slip with respect to the base frequency:

$$\frac{d^2\theta}{dt^2} = \frac{d}{dt}(\omega_m - \omega_b) = \frac{T_{mech} - T_{el} - (\omega_m - \omega_b) * DAMP}{2H} \qquad (D-17)$$

where θ is the rotor angle measured with respect to the magnetic axis of the three-phase stator windings, T_{mech} is the mechanical torque, H is the total inertia constant, and DAMP is a damping factor.

The rotor angle is equal to:

$$ANGLE = \omega_b * \int \frac{d}{dt}(\omega_m - \omega_b)dt + ANGLE_{INIT} \qquad (D-18)$$

The differential and algebraic equations above define the model for the single cage wound rotor induction machine.

Figure 2-3[1] shows the formulation of the model in the synchronous reference frame.

The equations and block diagram for the double cage wound rotor induction machine could be derived in a similar manner.

[1] de Mello, F.P., "Modeling of Induction Machines," Siemens PTI Course Notes, 2001.

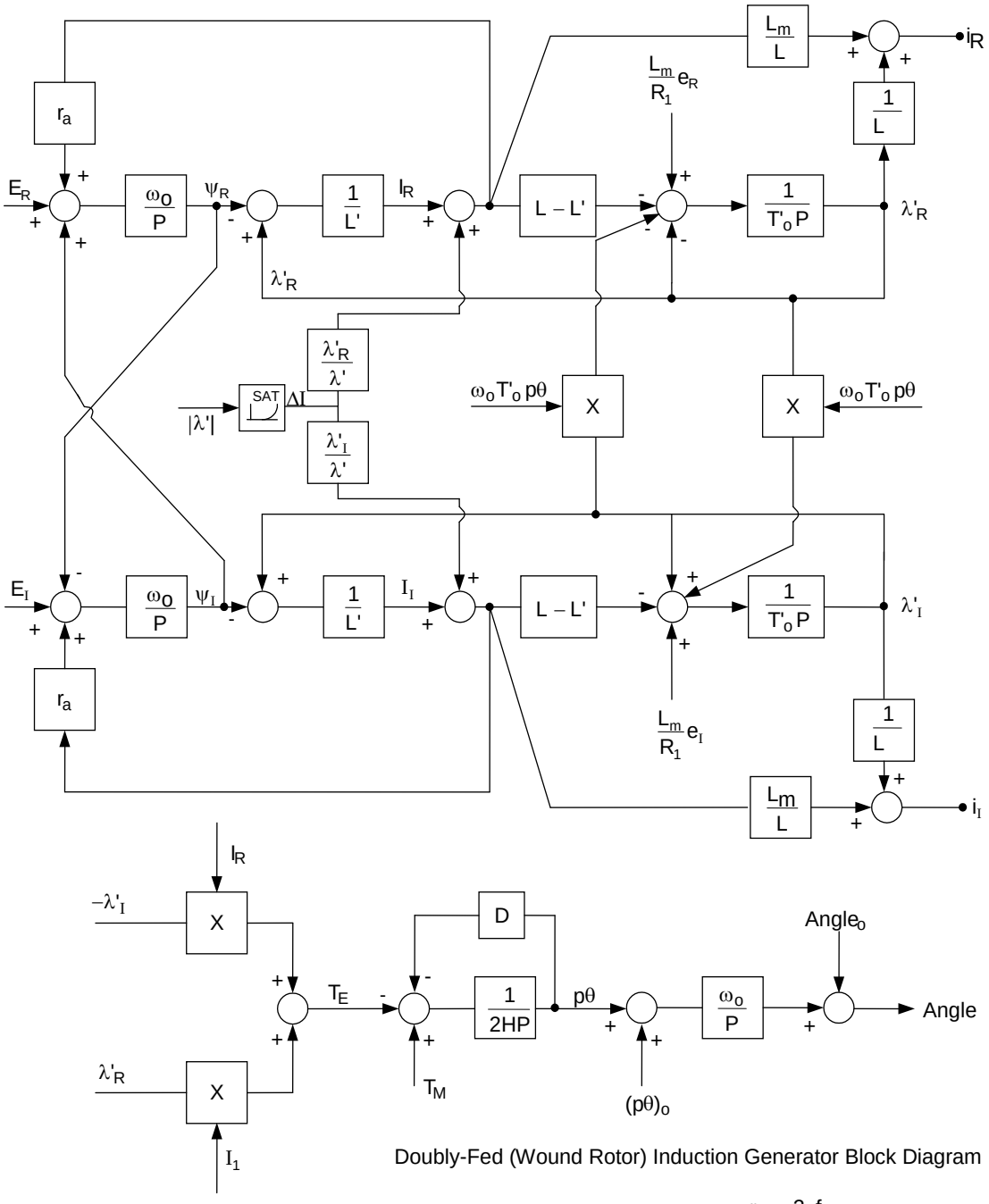

Doubly-Fed (Wound Rotor) Induction Generator Block Diagram

ψ stator flux linkage
λ' transient flux linkage
E, I stator voltage, current
e, i rotor voltage, current

$\omega_o = 2\pi f$

$T'_o = \frac{L}{\omega_o R_1}$

p - Laplace operator

Figure 2-3 Block Diagram for the Single Cage DFIM

2.1 Steady-State Theory

Steady-state equations can be derived by setting the dλ/dt terms from the voltage equations to zero:

$$v_{ds} = -R_s i_{ds} - \overline{\omega}_s \lambda_{q_s}$$
$$v_{qs} = -R_s i_{qs} + \overline{\omega}_s \lambda_{d_s}$$
$$v_{dr} = R_r i_{dr} - s\overline{\omega}_s \lambda_{q_r}$$
$$v_{qr} = R_r i_{qr} + s\overline{\omega}_s \lambda_{d_r}$$

These equations can be rewritten by introducing the following phasors or quantities:

$$\dot{V}_s = v_{ds} + jv_{qs}$$
$$\dot{V}_r = v_{dr} + jv_{qr}$$
$$\dot{I}_s = i_{ds} + ji_{qs}$$
$$\dot{I}_r = i_{dr} + ji_{qr}$$
$$\dot{\lambda}_s = \lambda_{ds} + j\lambda_{qs}$$
$$\dot{\lambda}_r = \lambda_{dr} + j\lambda_{qr}$$

Then, the equations for steady-state voltages and flux linkages will be as follows:

$$\dot{V}_s = -R_s \dot{I}_s + j\varpi_s \dot{\lambda}_s$$
$$\dot{V}_r = R_r \dot{I}_r + js\varpi_s \dot{\lambda}_r$$
$$\dot{\lambda}_s = -L_{ss} \dot{I}_s + L_m \dot{I}_r$$
$$\dot{\lambda}_r = -L_m \dot{I}_s + L_{rr} \dot{I}_r$$

or

$$\dot{V}_s = -R_s \dot{I}_s + j(-X_{ss} \dot{I}_s + X_m \dot{I}_r)$$
$$\dot{V}_r = R_r \dot{I}_r + js(-X_m \dot{I}_s + X_{rr} \dot{I}_r)$$

or

$$\dot{V}_s = -R_s \dot{I}_s - jX_1 \dot{I}_s - jX_m (\dot{I}_s - \dot{I}_r)$$
$$\dot{V}_r = R_r \dot{I}_r - jsX_m (\dot{I}_s - \dot{I}_r) + jsX_2 \dot{I}_r$$

where

$$X_1 = X_{ss} - X_m$$
$$X_2 = X_{rr} - X_m$$

or

$$\dot{V}_s = -R_s\dot{I}_s - jX_1\dot{I}_s - jX_m(\dot{I}_s - \dot{I}_r)$$
$$\frac{\dot{V}_r}{s} = \frac{R_r}{s}\dot{I}_r - jX_m(\dot{I}_s - \dot{I}_r) + jX_2\dot{I}_r$$

The equivalent circuit shown in circuit a of Figure 2-4 fits these equations.

By substituting

$$\frac{R_r}{s} = R_r(1+\frac{1-s}{s}),$$

the equivalent circuit can be changed to the form shown in circuit b of Figure 2-4.

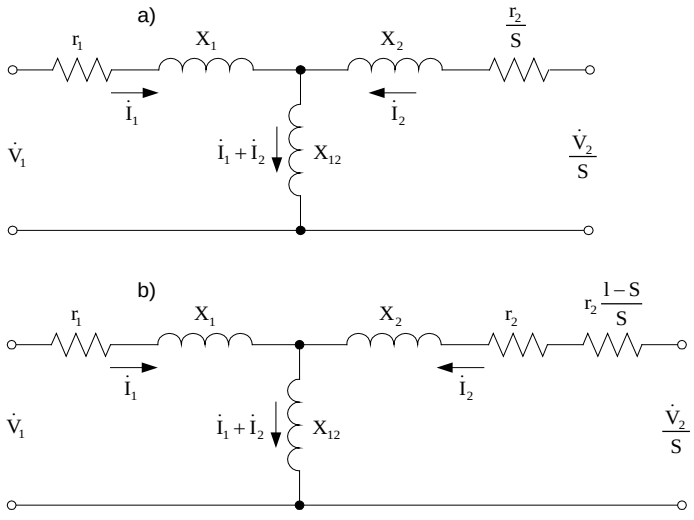

Figure 2-4 Equivalent Circuit of a Wound Rotor Induction Machine

In the last two diagrams, $V_1 = V_s$, and $V_2 = V_r$.

It is worth remembering that the notion of the equivalent circuit makes sense if dealing with phasors of the same fundamental frequency from both stator and rotor sides. Thus $V_1 = V_s$ and $V_2 = V_r$ are voltage phasors of the same frequency. To fit with the underlying physics and to obtain the correct value of the stator current which is of the fundamental frequency, we have to use not V_2 but V_2/s, and not r_2 but r_2/s.

Assuming $R_s = 0$, the complex stator and rotor currents can be derived as

$$\dot{I}_s = -\frac{(1+j\xi)\dot{V}_s - j\frac{X_m}{R_r}\dot{V}_r}{X_{ss}(j-\xi\sigma)}$$

$$\dot{I}_2 = -j\frac{\xi\frac{X_m}{X_{rr}}\dot{V}_s - \frac{X_{ss}}{R_r}\dot{V}_r}{X_{ss}(j-\xi\sigma)}$$

where

$$\sigma = 1-\mu = 1-\frac{X_m^{\ 2}}{X_{ss}X_{rr}}$$

$$\rho_2 = \frac{R_r}{X_{rr}}$$

$$\xi = \frac{s}{\rho_2}$$

For the sake of simplicity, the base voltage for the rotor is selected according to the ratio

$$\frac{V_{sbase}}{V_{rbase}} = \frac{X_m}{R_r}.$$

Then the expression for the stator current phasor can be rewritten as

$$\dot{I}_s = -\frac{(1+j\xi)\dot{V}_s - j\dot{V}_r}{X_{ss}(j-\xi\sigma)},$$

and electrical torque as

$$T_{el} = \mathrm{Re}(\dot{V}_s\dot{I}_s).$$

Assuming the stator voltage phasor as reference, then

$$\dot{V}_s = V_s,$$

that is, the phasor of the stator voltage is oriented along the real axis, R. The position of the phasor of the rotor voltage will then be displaced by the angle θ+90°; that is,

$$\dot{V}_r = V_r e^{j(\theta+\pi/2)}.$$

Then electrical torque can be found as

$$T_{el} = \frac{V_s V_r}{X_{ss}\sqrt{1+(\xi\sigma)^2}}\sin(\theta - \alpha) + \frac{V_s^2}{X_{ss}}\frac{\xi\mu}{1+(\xi\sigma)^2},$$

where α = atan($\xi\sigma$) is a function of the slip s.

The first term of T_{el} is a synchronous torque which at ξ = 0, that is, at s = 0, is equal to synchronous torque of the synchronous machine. The second term of T_{el} is the asynchronous torque identical to the electrical torque of the induction machine with a squirrel cage rotor.

Figure 2-5 parts 5a, 5b, and 5c show T_{el} versus θ characteristics for V_1/V_2 = 1.5, 1.0, and 0.5, respectively; σ = 0.2; and different values of ξ. One can see that, by virtue of the asynchronous component, a wound rotor induction machine can operate as a generator (T_{el} >0) for θ < 0 and as a motor for θ > 0.

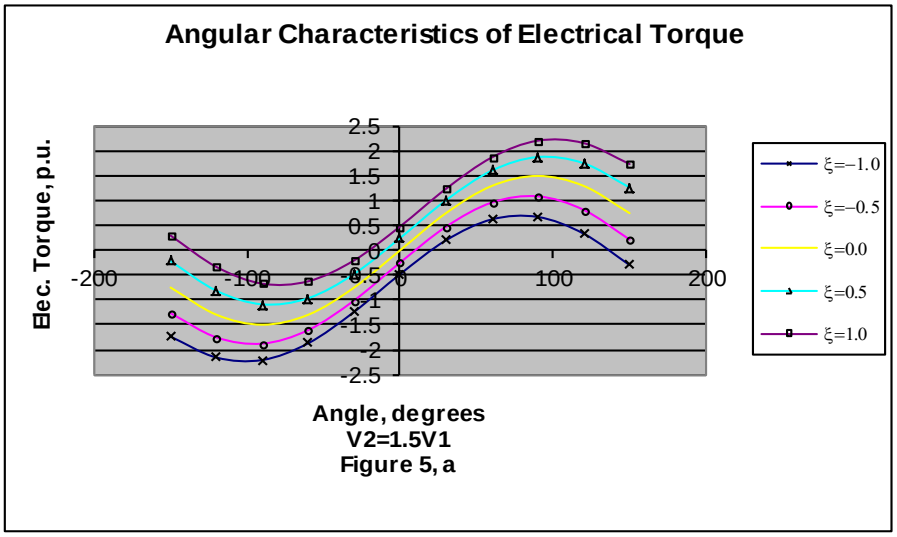

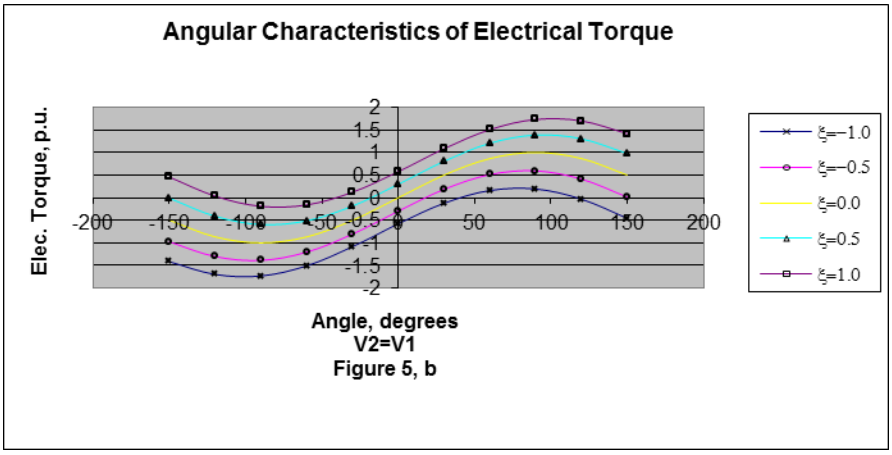

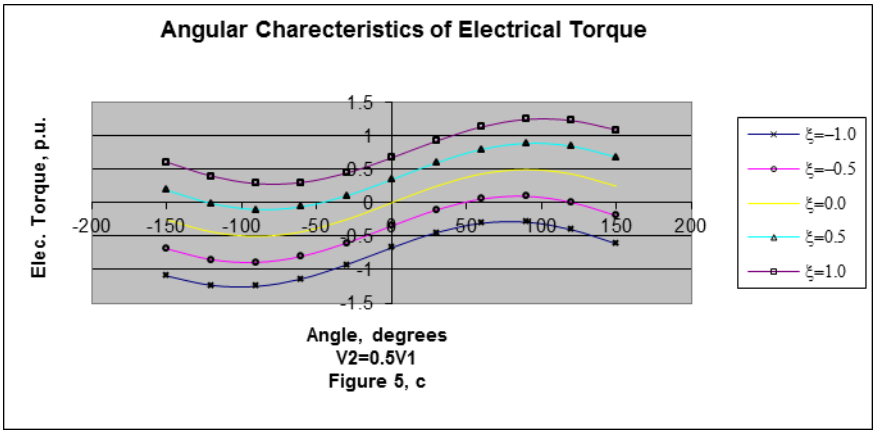

Figure 2-5 Electrical Torque Tel versus Phase Shift Angle θ for Ratios of Stator and Rotor Voltages V_1/V_2 = 1.5, 1.0, and 0.5, Respectively, with σ = 0.2 and Different Values of ξ

This page intentionally left blank.

Section
3

Modeling Units Employing a DFIM in PSS®E

3.1 The Detailed Model

On the basis of the theory described in Section 2, the PSS®E dynamic simulation model DFIGDC was developed to represent the double cage wound rotor induction machine. Figure 3-1 shows the model data sheet for the DFIGDC model.

Since the DFIGDC model includes the stator flux linkage dynamics, it fairly well represents the fundamental frequency or rotor slip frequency components and exponential components triggered by faults. The rotor controls are modeled by using a simplified, generic representation.

The characteristics of the model are demonstrated by its response to a series of tests. A 2-MW 50-Hz DFIM was modeled in these tests.

The power versus rotor speed characteristic of the DFIM used in these tests is shown in Figure 3-2. As seen in this figure, at rated power, the rated speed is 20% above synchronous speed. The DFIM was dispatched at 57% of its rated power for the tests. Therefore, the respective rotor speed was 6.67% above the synchronous speed. To demonstrate the characteristics of the machine (as compared to the characteristics of the controls), the rotor controls were disabled; that is, the rotor voltage d and q components were kept constant.

The plots in Figure 3-3 depict the machine terminal voltage and rotor speed response to a remote fault. It can be seen that voltage is maintained close to its initial value, and the speed of the unit exhibits a well-damped dynamic response.

Stator and rotor currents are shown in Figure 3-4. Note the presence of a high-frequency component as well as components at the same frequency that is seen in the plot of the rotor speed, that is, the typical inter-machine rotor angle oscillation frequency.

Figure 3-5 shows the same stator and rotor currents zoomed in for the one-second period starting from the fault inception. The higher frequency component now can be clearly seen. The frequency of this component is related to the rotor slip (in this case

Siemens PTI

Nonstandard Model Data Sheet
DFIGDC

DOUBLY-FED (WOUND ROTOR) INDUCTION MACHINE WITH THE POWER CONVERTER ROTOR CONTROL

This model is located at system bus #_____IBUS
Machine #_____I
This model uses CONs starting with #_____J
and STATEs starting with #_____K
and VARs starting with #_____L
and ICONs starting with #_____M

CONs	#	Value	Description
CONs of the Main Program			
J			Ra, Stator resistance, pu
J+1			La, Stator Inductance, pu
J+2			Lm, Mutual Inductance, pu
J+3			R1, Rotor Resistance, pu
J+4			L1, Rotor Inductance, pu
J+5			H, total drive train inertia, sec.
J+6			D, Damping Factor, pu
J+7			E1, Saturation Parameter, pu
J+8			S(E1), Saturation Parameter, pu
J+9			E2, Saturation Parameter, pu
J+10			S(E2), Saturation Parameter, pu
CONs of the Control Program			
J+11			KP2, P-gain of PI Control, pu
J+12			KI2, I-gain of PI Control, pu
J+13			KP3, Gain of Voltage Control, pu
J+14			KI3, gain of Voltage Control Integral, pu
J+15			IRMAX, Rotor Current Limit, pu
J+16			VRMAX, Rotor Voltage Limit, pu
J+17			SMAX, Total Converter Power Limit, pu
CONs of the Power Curve Program			
J+18			Init. Power Limit
J+19			Init. Speed Limit
J+20 to J+49			Coordinates of the Power vs Rotor Speed Characteristic

STATEs	#	Description
STATEs of the Main Program		
K		Psi_d, Stator Flux Linkage, pu
K+1		Psi_q, Stator Flux Linkage, pu
K+2		Lambda_d_prim, rotor transient flux linkage, pu
K+3		Lambda_q_prim, rotor transient flux linkage, pu
K+4		Rotor Speed Deviation, pu
K+5		Rotor Angle deviation, degrees
STATEs of the Control Program		
K+6		Q-axis PI
K+7		D-axis Integrator
K+8		D-axis PI

VARs	#	Description
VARs of the Main Program		
L		Ed, Rotor Voltage, pu on MBASE
L+1		Eq, Rotor Voltage, pu on MBASE
L+2		Rotor Speed, pu
L+3		Rotor Slip, pu
L+4		Id, Stator Current, pu on MBASE
L+5		Iq, Stator Current, pu on MBASE
L+6		RTR_P, Rotor Real Power, pu on MBASE
L+7		RTR_Id, Rotor Current, pu on MBASE
L+8		RTR_Iq, Rotor Current, pu on MBASE
L+9		Initial Machine Internal Angle (rads)
L+10		Initial Slip, pu
L+11		Initial Mechanical Torque, pu
VARs of the Control Program		
L+12		TSP Proportional Factor

ICONs	#	Description
ICONs of the Main program		
M		Memory

IBUS, 'USRMDL', I, 'DFIGDC', 1, 1, 1, 50, 9, 13, 0, CONs from (J) to (J+49) /

Notes:

1. The wind power to speed curve is approximated by 15 pairs of data points consisting of the rotor speed in p.u. with respect to the synchronous speed and the total real power of the machine in p.u. of MBASE.

Figure 3-1 Model Data Sheet for the DFIGDC Model of the Doubly-Fed Induction Machine

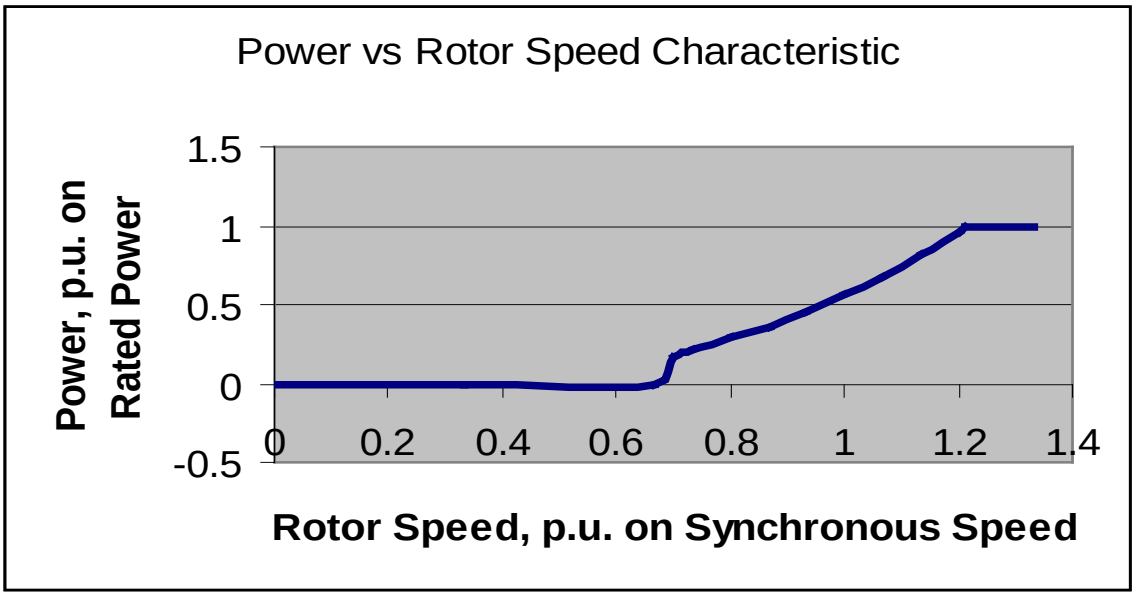

Figure 3-2 Steady-State Power versus Rotor Speed Characteristic of the DFIM Used in the Tests

53 Hz = synchronous speed of 50-Hz frequency times 1.067, the overspeed determined by the power versus rotor speed characteristic of Figure 3-2. Note that the higher frequency component is also well damped.

The model allows simulation of a single cage machine by setting the rotor inductance L1 to a very high value, for example, 99999 per unit. It is noteworthy that, although possible, it is not very likely that one would encounter a DFIM with two rotor windings.

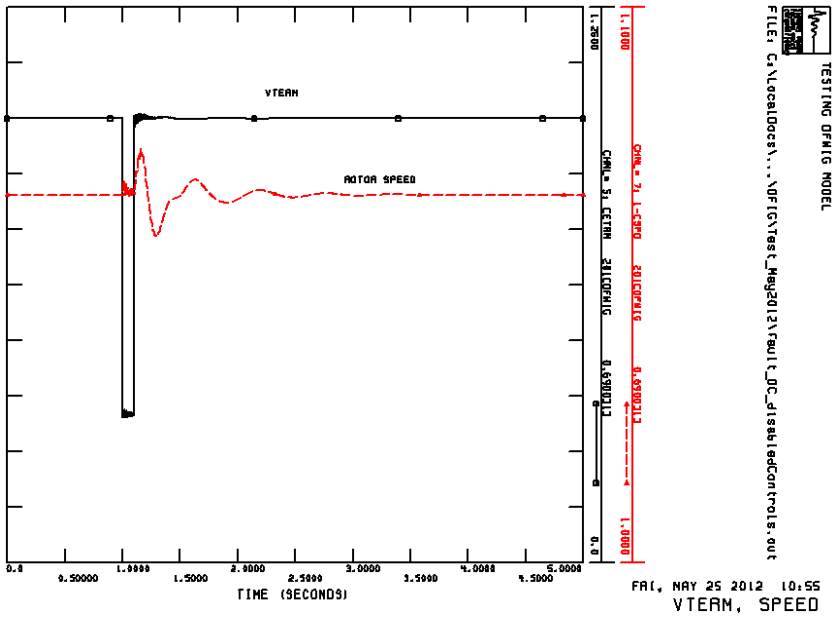

Figure 3-3 Response of DFIM Terminal Voltage and Rotor Speed to a Remote Fault

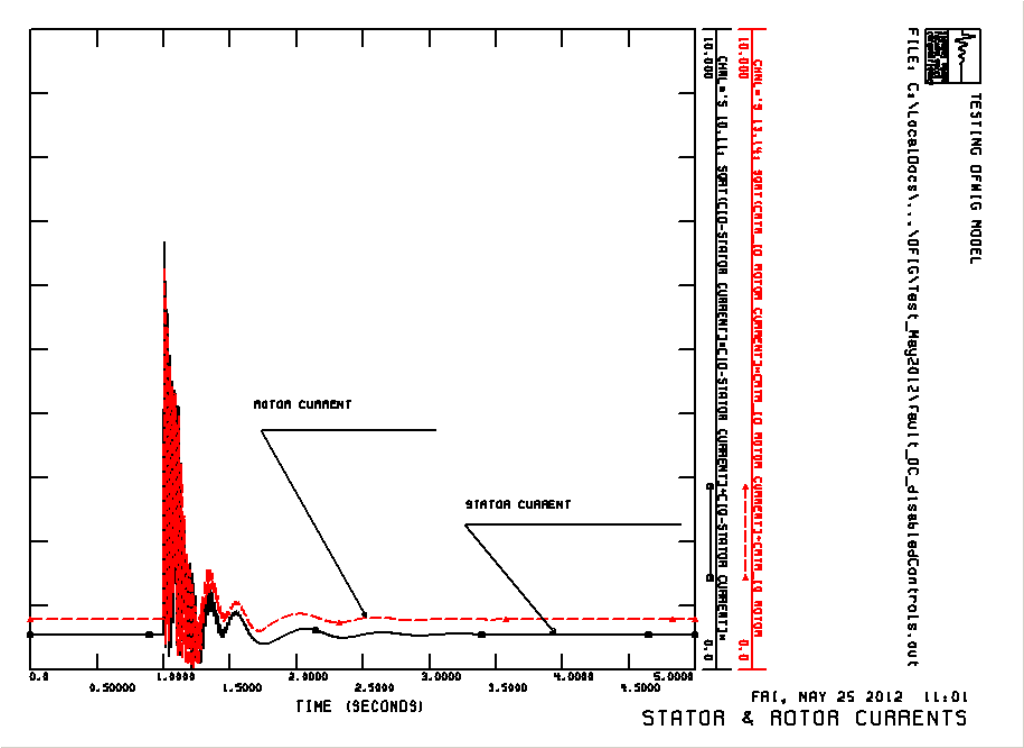

Figure 3-4 Response of DFIM Stator and Rotor Currents to a Remote Fault

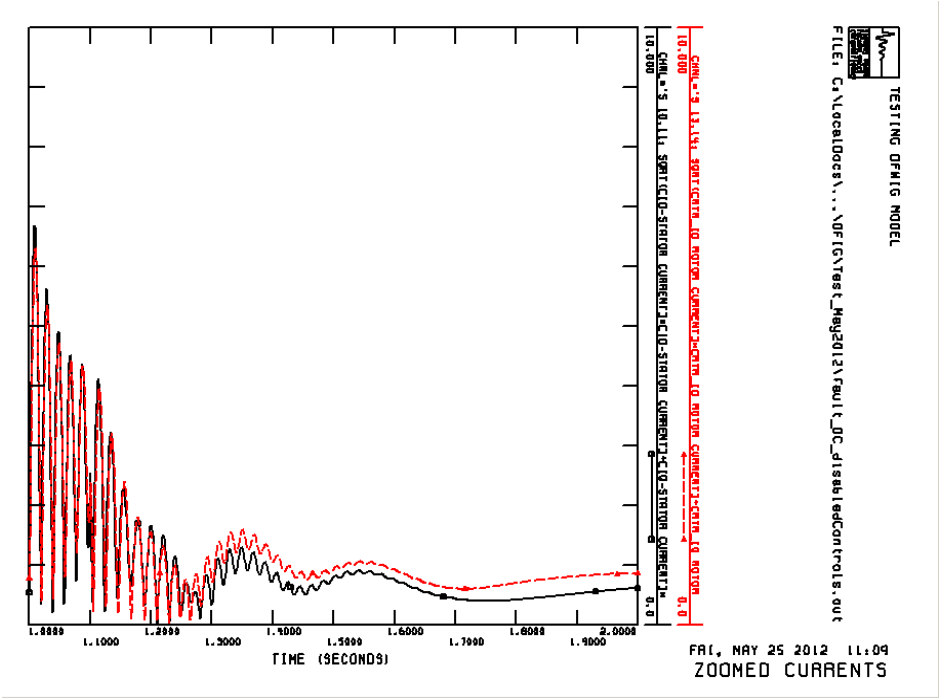

Figure 3-5 Response of DFIM Stator and Rotor Currents Zoomed in to Show Response in the One-Second Period Following the Remote Fault

3.2 The Simplified Model

The full order model described above is not appropriate for stability studies because it requires a significant reduction of the integration time step. Moreover, it is well known that taking into account the stator flux linkage dynamics is not necessary for stability studies. However, the rotor flux linkage dynamics must be represented in the electrical machine model used for rotor angle and voltage stability studies.

The PSS®E dynamic model library contains several models of induction generators; for example, the CIMTR3 and CIMTR4 models. These models include both the rotor flux dynamics and the inertial dynamics, but not stator flux dynamics. The plots in Figure 3-6 show the dynamic response of the CIMTR3 and DFIGDC models to a system disturbance. Three key variables are shown: machine terminal voltage (Vterm), active power (Pelec), and reactive power (Qelec). This plot clearly demonstrates that the CIMTR3 model provides good accuracy in representing the average component of these variables, which is sufficient for rotor angle and voltage stability studies.

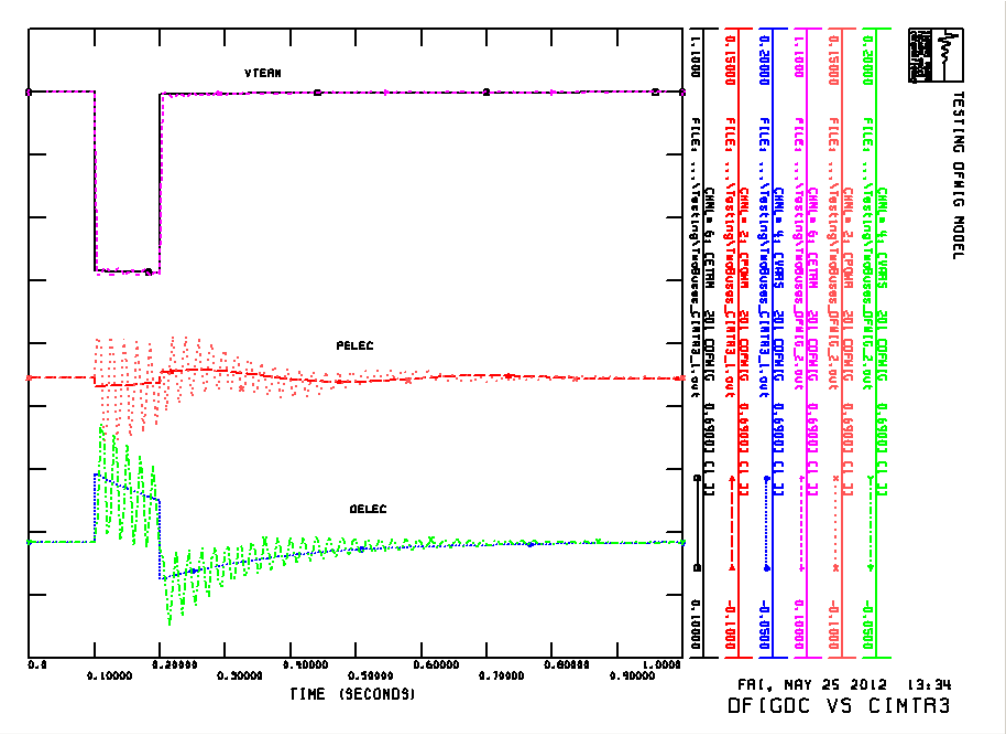

Figure 3-6 Comparison of the Response of the DFIGDC Model and the Standard CIMTR3 Induction Motor Model

The vector control provided by a power converter connected to the rotor of the DFIM processes commands in terms of d (R) and q (I) components of rotor current responsible for controlling the machine voltage across the magnetizing branch and electromagnetic torque. This control is done in a very fast manner by means of high-frequency PWM electronics. The rotor current follows these commands with negligible delay. As currents of the rotor and stator are closely related, the current injected by the DFIM into the grid

may be determined also based on the commands issued by these controls. This fundamental consideration allows us to dramatically change the approach to modeling of the DFIM controlled by a power converter connected to its rotor winding. The model should have a fair representation of the controls whose outputs are applied to a combined machine/converter model, but it does not need to model either the very fast PWM electronics or include a detailed model of the machine.

This philosophy has been successfully employed for modeling DFIM wind turbines. It can be illustrated with the control structure used in the generic WT3 wind turbine model.[2] It is worth mentioning that the implementation of this model in the two most widely used commercial stability simulation software packages, PSS®E and Positive Sequence Load Flow (PSLF), is identical.

Figure 3-7 shows the signal flow diagram of the DFIM-based wind turbine model and demonstrates how the modules of the different elements interact with each other. The aerodynamic mechanical power P_{mech} is calculated based on the turbine blade's pitch angle. The wind turbine model calculates the DFIM rotor speed deviation by using the difference between the prime mover P_{mech} and the active power P_{gen} returned by the generator/converter module. The generator/converter module gets inputs from the converter control module in the form of an active current command and the voltage across the magnetizing branch command.

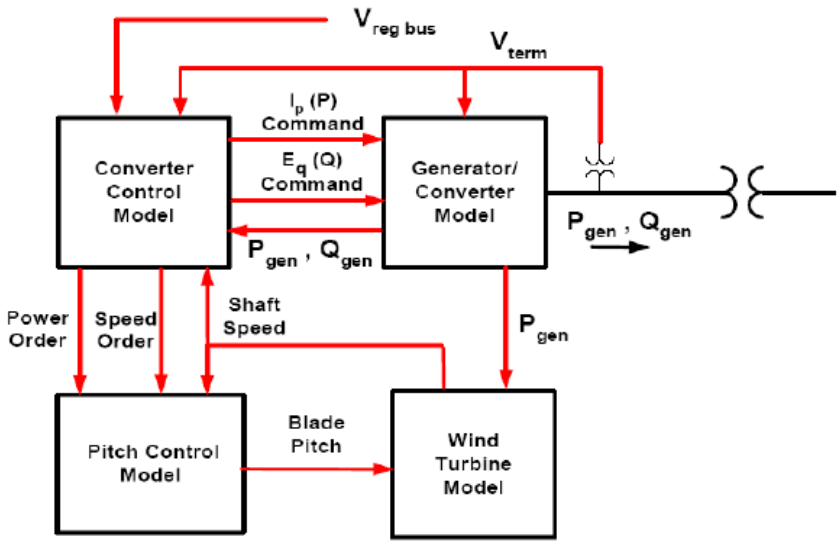

Figure 3-7 Signal Flow Diagram of the DFIM-Based Wind Turbine Model

The active power (electromagnetic torque) control block diagram is shown in Figure 3-8. The DFIM rotor speed is an input to this model. The rotor speed reference is provided by a lookup table f(P_{gen}) with active power as the input. This lookup table actually

[2] Ellis, A., E. Muljadi, J. Sanchez-Gasca, and Y. Kazachkov, "Generic Models for Simulation of Wind Power Plants in Bulk System Planning Studies," IEEE paper 2011GM1462, IEEE PES Annual Meeting, Detroit, MI, July 2011.

reproduces the so called “Power-Rotor speed” characteristic that is unique for each type of unit. The rotor speed error is processed through a PI controller and a first order delay that has the power order as output. This output divided by the machine terminal voltage produces the active current command, $I_{p\ cmd}$.

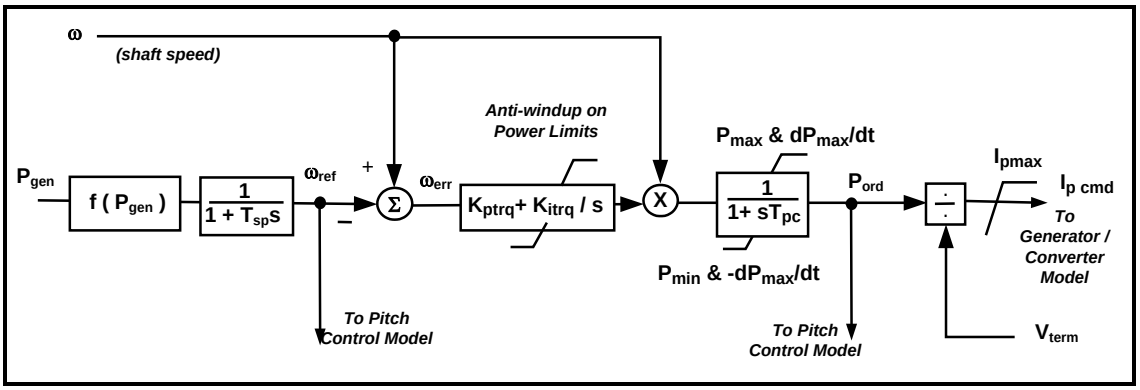

Figure 3-8 Active Power (Electromagnetic Torque) Control Block Diagram

The reactive power control block diagram is shown in Figure 3-9. The reactive power command Q_{cmd} may come from an external model that may be responsible for the remote bus voltage control or power factor control. The reactive power error, the mismatch between the reactive power command and the machine generated reactive power, is the input for the integral control whose output is the terminal voltage reference. The terminal voltage error is integrated, and the output of the integral controller is the internal voltage command $E_{q\ cmd}$.

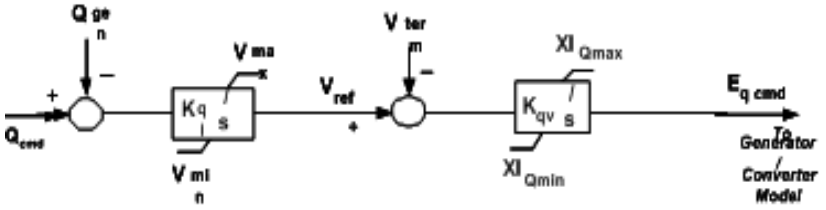

Figure 3-9 Reactive Power Control Block Diagram

Both Ip_{cmd} and Eq_{cmd} from the uncoupled active and reactive power controls are input to the generator/converter model whose simplified example is shown in Figure 3-10. Two first-order lags with small time constants simulate the electromagnetic dynamics of the machine. This model also includes the mechanical dynamics of the rotor.

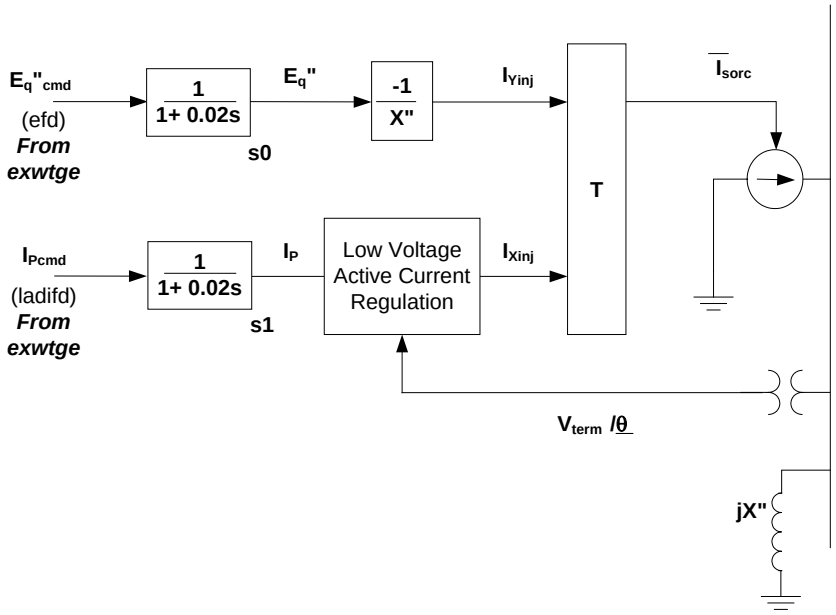

Figure 3-10 Generator/Converter Model

Section

4

Modeling Adjustable Speed Drive Hydro Pumped Storage Units Employing a DFIM

The modeling of wind turbines employing a DFIM was described in Section 3 to explain the pertinent mathematics and the lessons learned in the long evolution of these models into their presently well-accepted versions. While there are obviously differences between the modeling requirements of those wind units and of PSH units employing a DFIM, there are also many similarities. For example, the required level of modeling of the machine was thoroughly investigated for the wind turbines, and this knowledge can be applied to the modeling of these pumped storage units. General control strategies can also be adapted. For example, the wind turbine's aerodynamic mechanical power P_{mech} is calculated based on the turbine blade's pitch angle; this can be thought of as analogous to the gate position control used in a hydro application. Also similar to the approaches taken in the wind application, some control functionalities cannot be taken into account in the positive sequence fundamental frequency phasor approach typical for the stability studies; thus, these functionalities also will be ignored in the PSH modeling. An example of this is the well-known crowbar control used for protecting the converter equipment.

The recommended model structure for a PSH unit employing a DFIM is given in this section. The design of this model draws heavily on the control structures described in a paper by T. Kuwabara, A. Shibuya, and H. Furuta titled "Design and Dynamic Response Characteristics of 400 MW Adjustable Speed Pumped Storage Unit for Ohkawachi Power Station" (IEEE Transactions on Energy Conversion, Vol. 11, No. 2, June 1996). We found the approach to modeling—which is based on the experience of these Japanese authors that was gained at their Ohkawachi PHS plant — to be the most practical and useful of the many references reviewed. It is also consistent with our understanding and the modeling practices of commercial stability programs. However, there are many other references and ongoing development efforts, thus the selection of this control structure is not to be construed as indicating that other potential control structures are impossible, since they may have advantages for particular installations or technologies.

The control structure selected reflects a thorough review of the literature. Two primary approaches to control are described in the reviewed literature, based on the two primary variables to be controlled.

In a conventional pumped storage plant, synchronous machines are employed. The input to the governor controls is speed, and the gate position is controlled to adjust power. The machine speed is not controlled; since the machine is a synchronous machine, speed is locked to the system frequency.

In a pumped storage plant employing a DFIM, there are two controllable variables: gate position and speed, as the speed of the machine is no longer locked to system frequency. In the steady state, the controls select the optimum relationship between gate position and speed to get the desired power. However, there are three basic control approaches:

1. The electrical power is controlled by the power converter, and the rotating speed is controlled by the turbine governor adjusting the gate position.
2. The rotating speed is controlled by the power converter, and the electrical power is controlled by the turbine governor adjusting gate position.
3. A combination of these two approaches.

Since the power converter can be adjusted very quickly (tenths of a second) compared to gate position (seconds), control strategy 1 above is labeled as Fast Power Control and control strategy 2 as Fast Speed Control. In a general sense, it can be shown that both approaches work, although the transient response of the units to events occurring on the system is very different.

The control investigations that are related to the design of the Okhawachi power plant in Japan showed the response employing both control strategies.[3] The authors show that Fast Power Control is a superior approach compared to Fast Speed Control. They conclude that a DFIM pumped storage unit with Fast Power Control would exhibit a transient behavior superior to a unit with a synchronous machine, while a DFIM unit with Fast Speed Control would exhibit a transient behavior inferior to a unit with a synchronous machine.

The two control strategies are also compared in another reference.[4] The authors conclude that the Fast Speed Control strategy is detrimental to grid stability. This is illustrated by the simulation of an event calling for a reduction in power (in this case, a step reduction in the active power set point). It is shown that the speed is quickly controlled to the new desired setting, but the power injected by the unit into the grid actually goes in the opposite direction and increases initially and decreases only after several seconds. The authors state that the transient behavior resulting from the variation is not acceptable. They then show that the Fast Power Control strategy is capable of following changes of the power set point very quickly, about 84 times quicker than using the alternate strategy, and it results in very acceptable transient behavior.

[3] Nagura, O., and M. Yoshida, “Transient Behavior Analysis of Adjustable Speed Pumped Storage System,” Hydro Vision International 2011, Session# 414; Sacramento, CA; July 20, 2011.

[4] Pannatier, Y., et al., “Transient Behavior of Variable Speed Pumped-Turbine Units,” IAHR, 24th Symposium on Hydraulic machines and Systems, October 2008.

The findings of the fifth reference[5] are based on the experience gained at the Goldisthal pumped storage plant in Germany. Similar to the previous references, both control strategies were investigated. The Fast Power Control strategy was shown to be superior and was selected as the preferred strategy.

There are other PSH plants, such as the Yagisawa and Shiobara plants in Japan, where the third control strategy is employed, using a combination of control strategy 1 (Fast Power Control) and strategy 2 (Fast Speed Control).[6] The output power of these units is normally controlled by adjusting the guide vane opening, and the converter controls adjust to maintain the optimal rotating speed. This is essentially strategy 2. However, in the case of a large disturbance casing a significant frequency deviation, the controls respond very quickly due to an additional compensation signal applied to both the converter control and the gate controls. Thus for large disturbances, the response of strategy 3 will be similar to strategy 1, because both of these control strategies adjust the electrical output not only by mechanical input (gate control) but also by using the inertia of the rotating mass (through power control by the converter). The stated advantage of this approach is that it meets both electrical and mechanical requirements in that it reduces the movement of the guide vane and the adjustment of the rotating speed of the units, while still maintaining the ability to make a quick response under conditions where it is needed.

In the modeling effort described below, the Fast Power Control strategy is employed.

4.1 Turbine Mode of Operation

Figure 4-1 shows the control diagram suggested for the turbine (generating) mode of operation. This figure shows the general control scheme and the connection between the many components of the control structure. Each of these components will be further explained below.

[5] Kopf, E., et al., “Optimized Control Strategies for Variable Speed Machines,” 22nd IAHR Symposium on Hydraulic Machinery and Systems, June 2004.

[6] Communications with Teruyuki Ishizuki of Toshiba Corporation, Japan.

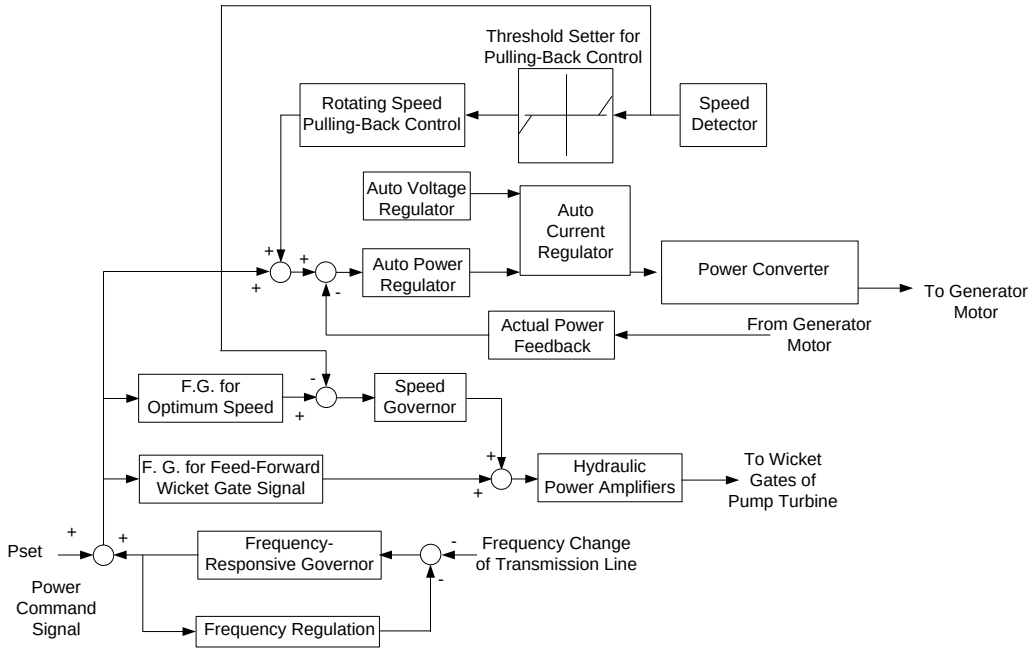

Figure 4-1 Control Scheme of Adjustable Speed Machine in Generator Mode

The converter control is responsible for controlling active power and voltage.

The power command is combined with the command from the frequency control as shown in Figure 4-2. The total power command is P_{set}.

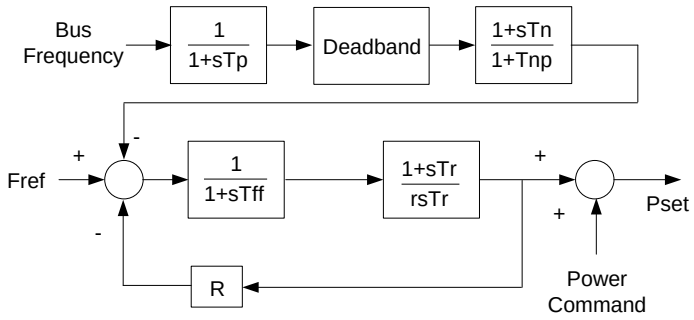

Figure 4-2 Frequency Responsive Governor Control

The total power command P_{set} is summed up with the “Rotating Speed Pulling-back Control.” The purpose of the latter is to make sure that the machine’s speed never goes beyond the predetermined lower and upper limits that are determined by the size of the converter.

The power error is processed by a PI regulator. Then the active current command, along with the reactive current command from the voltage regulator, is fed to the power converter control.

The turbine governor is controlling the machine shaft speed. The total power command P_{set} enters the “Speed Optimizer” whose output is the speed reference. The speed error is the input for the hydro turbine speed governor.

Figure 4-3 shows the signal flow diagram of the model for turbine operation.

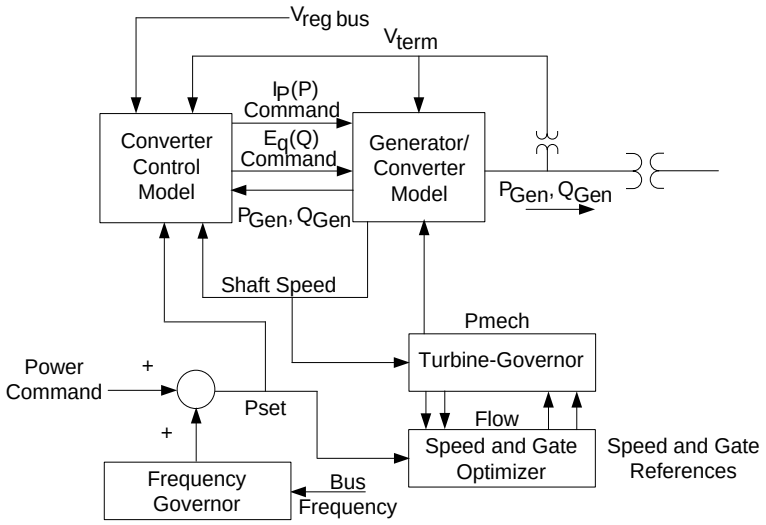

Figure 4-3 Connectivity Diagram for the Turbine Mode of Operation

Specific controllers are shown below. Figure 4-4 shows the active power controller that supplies the power reference to the generator/converter module.

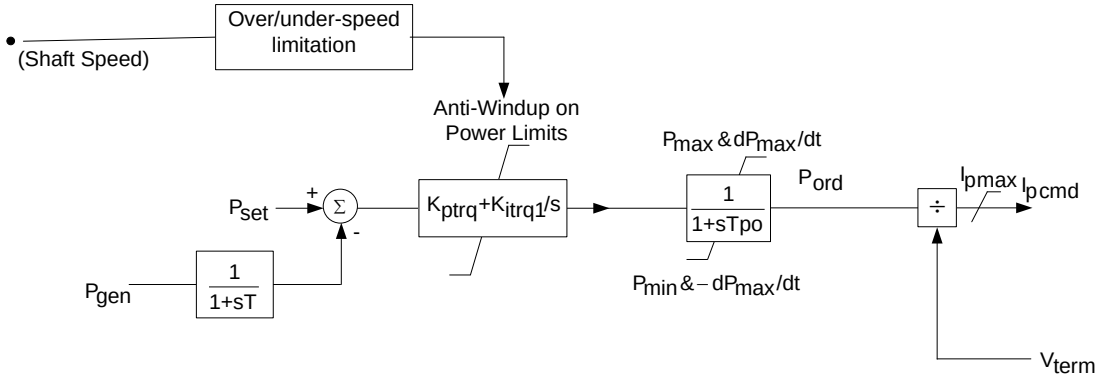

Figure 4-4 Active Power Controller for the Turbine Mode of Operation

Figure 4-5 shows the model for the governor, turbine, and penstock dynamics. While the model of the physics of the turbine and penstock are similar to that of conventional hydro units, this model addresses the extra degree of freedom in control of the adjustable speed unit. The mechanical power can be adjusted by either a change in turbine speed or in a change in gate position or in a combination of both. The speed and gate optimizers select the proper coordination of speed and gate position to maximize efficiency. Note that the optimization process itself is not modeled; however, the optimal

mechanical power/gate/speed relationships supplied by the manufacturer are represented through simplified functional characteristics. The model also includes provision for simulating hydraulic coupling effects for units sharing the same penstock.

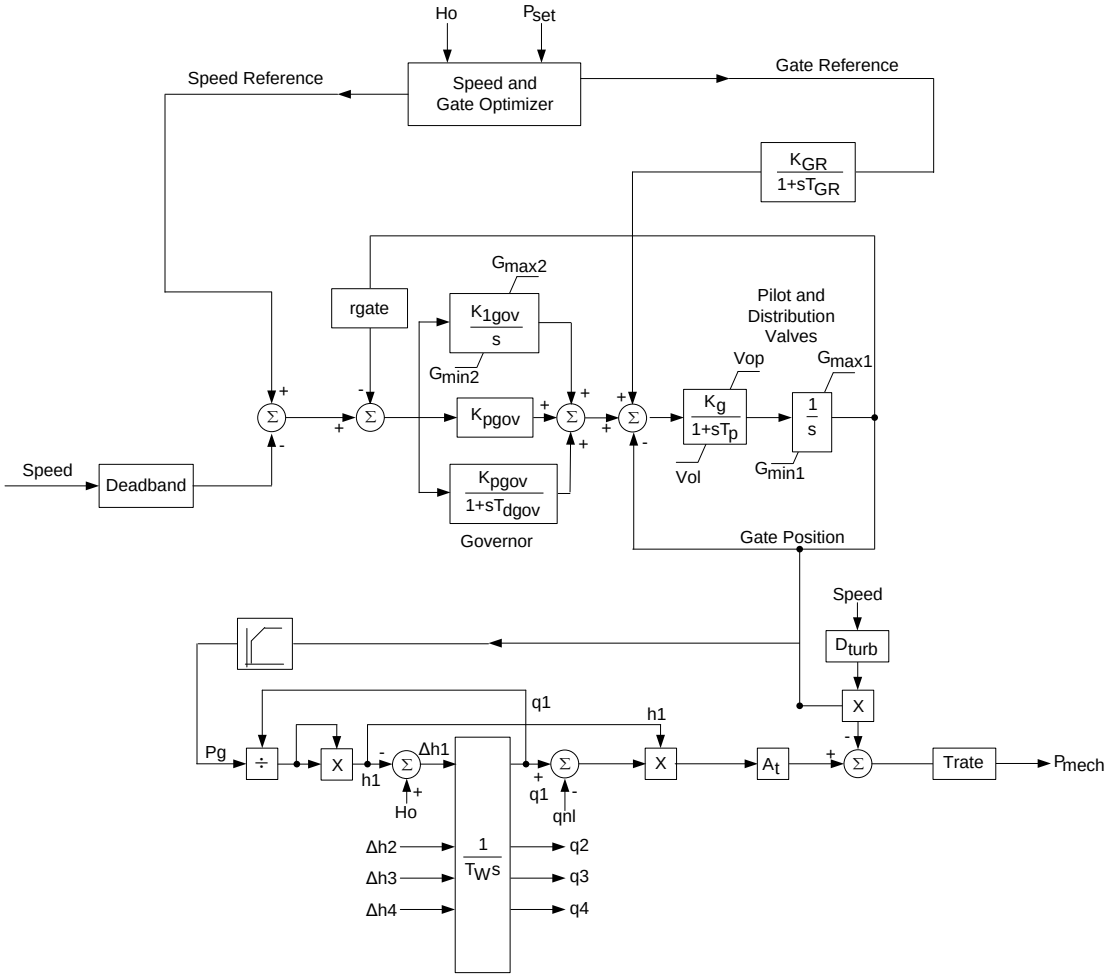

Figure 4-5 Governor, Turbine, and Penstock Dynamics Model for the Generating Mode

Figure 4-6 shows the generator/converter model. The power reference from the active power controller and the voltage reference from the reactive power controller (described below) are used to determine the desired current command; and thus, the desired generator active and reactive power. The generator/converter model also includes the rotor inertial dynamics as shown in Figure 4-6.

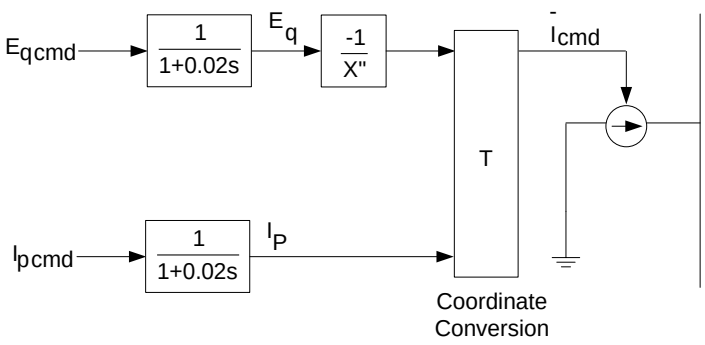

Figure 4-6 The Generator/Converter Model

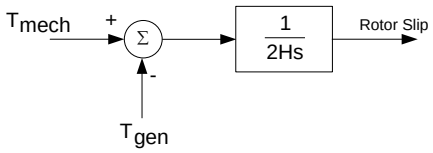

Figure 4-7 Inertial Dynamics of the Generator/Converter Model

Figure **4-8** shows the reactive power controls. The voltage of the regulated bus is controlled to the voltage reference by the PI controller. The PI controller determines a voltage reference which is passed to the generator/converter controls.

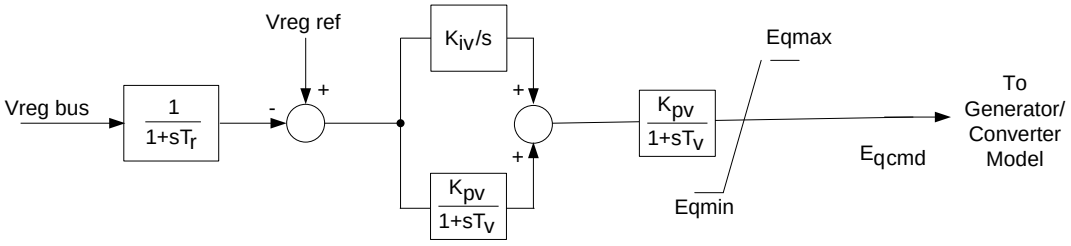

Figure 4-8 Reactive Power Controller for the Turbine Mode of Operation

4.2 Pumping Mode of Operation

The following control diagrams are suggested for modeling the pumping mode of operation. The control scheme is similar to that used for the generating mode but has some significant differences. Figure 4-9 shows the general control strategy. Figure 4-10 shows the control structure and the linkages between its many components. The components that are different from those described above for the generating mode will be further explained below.

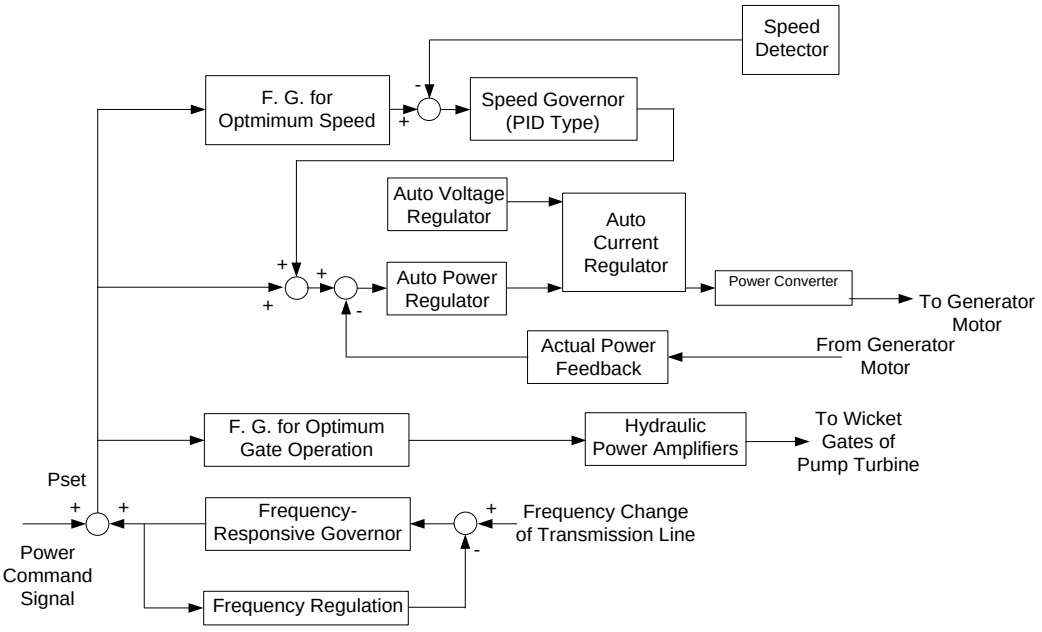

Figure 4-9 Control Scheme of Adjustable Speed Machine in Pump Mode

As in the generating mode, the converter control is responsible for controlling both active power and voltage. The major differences from the generating model are in the active power controller and the modeling of the physics of the gate, pump, and penstock relationships.

Figure 4-11 shows the active power controller in the pump mode. The desired speed at power P_{set} is determined from the speed optimizer and compared to the actual speed. A PI controller determines the desired power, which is then compared to the power absorbed by the unit, and then another PI controller determines the active current command. The active current command, along with the reactive current command from the voltage regulator, is fed to the power converter control.

The total power command P_{set} is also used by the gate optimizer to determine the desired gate position. Figure 4-12 shows the model of the gate, pump, and penstock dynamics.

The generator/converter controls and the reactive power controls are identical to those documented above for the turbine mode of operation.

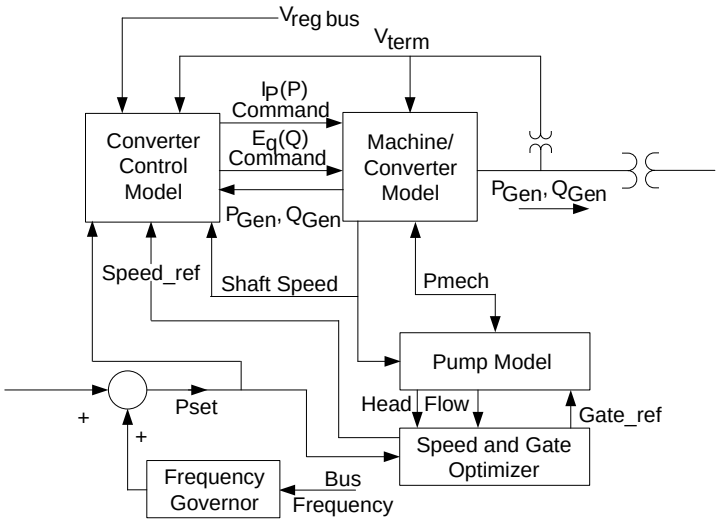

Figure 4-10 Connectivity Diagram of the Model for the Pump Operation

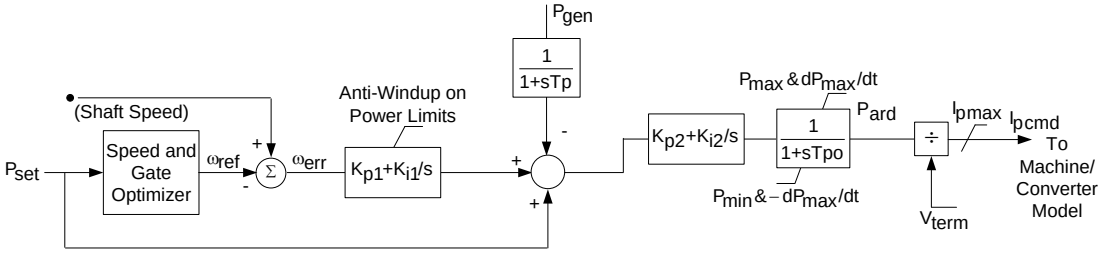

Figure 4-11 Active Power Controller for the Pump Mode of Operation

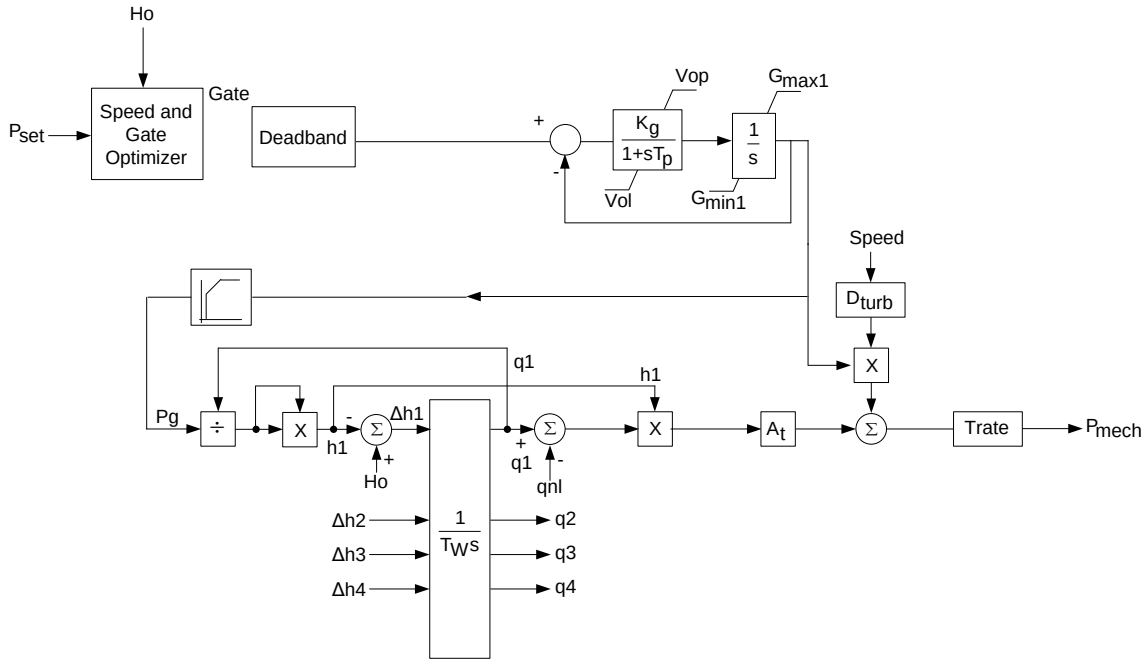

Figure 4-12 Model for Gate, Pump, and Penstock

4.3 Rotor Speed/Gate Position Relationships

The basic physics of the pump/turbine and penstock for an adjustable speed machine are similar to the physics of conventional PSH units. However, a conventional unit operates at synchronous speed; and thus, the only controllable quantity is gate position. In the generating mode, the power output of the unit is controlled by adjusting the gate position. Of course, throttling the flow through the closing of the gate has an impact on efficiency. In the pumping mode, the impact on efficiency would be even greater, as closing the gate would result in an increase of the effort required to pump a given amount of water. Thus, conventional units generally operate at a wide-open gate in the pumping mode at a fixed pump load.

With an adjustable speed pumped storage unit, both speed and gate position can be controlled. Of course, this results in an additional need to determine the optimal settings for these two interrelated quantities. Manufacturers have detailed models and computer programs that calculate the efficiency in generating or pumping mode. These calculations result in a “hill” diagram that shows efficiency for a range of gate, speed, and flow (or gate, speed, and power) at a given static head. These diagrams can be used to determine the gate and speed which give the best efficiency for a given static head and flow rate (or power at a given static head).

The model does not need to contain these complex optimization calculations. The speed and gate optimizers of the model will be used to select the proper coordination of speed and gate position to maximize efficiency. While the optimization process itself is not

modeled, the optimal mechanical power/gate/speed relationships supplied by the manufacturer are represented through simplified functional characteristics.

Some publications suggest examples of optimal characteristics obtained as a result of calculations or tests. Harbort et al. (1998) shows a performance graph that provides the optimal speed as a function of the MW output and the water head. A possible range of rotor speed determined by the size of the power converter is marked as ±15%. The performance graph shows that for a given power, the optimal speed is almost indifferent to the water head for the three values of static head shown (a variation of more than 10%).

Based on the performance graph for optimal turbine speed, it is also possible to obtain optimal gate opening function (Harbort et al, 1998). This function shows the gate opening's dependence on power and water head for the optimal speed.

Note that the model of the PSH unit described above will not be project specific. A big challenge of this project is to develop these functions as generic lookup tables that can be used for simulating the performance of any commercially available hydro unit.

This page intentionally left blank.

Section
5

Bibliography

Numerous publications are available on different aspects of variable speed hydro pumped storage units. The most relevant ones for the purpose of this study are provided here.

1. Kuwabara, T., A. Shibuya, and H. Furuta, "Design and Dynamic Response Characteristics of 400 MW Adjustable Speed Pumped Storage Unit for Ohkawachi Power Station," *IEEE Transactions on Energy Conversion*, Vol. 11, No. 2, June 1996.

2. Kita, E., A. Bando, and T. Kuwabara, "400 MW Adjustable Speed Pumped Storage Hydraulic Power Plant," *Hitachi Review,* Vol. 44, No. 1, 1995.

3. Harbort, T., G. Lein, and E. Goede, "Power Frequency Control of a Pump Turbine as an Example for the Operation with Adjustable Speed of Hydraulic Machines," University of Stuttgart, 1998.

4. Pannatier, Y., C. Nicolet, B. Kawkabani, J.-J. Simond, and P. Allenbach, "Dynamic Behavior of a Two Variable Speed Pump-turbine Power Plant," *Proceedings of the 18th International Conference on Electrical Machines*, 2008.

5. Fujii, T., K. Mine, and O. Nagura, "Contribution of Adjustable Speed Pumped Storage System for Electrical Grid Stability," Presented at Hydro 2010, Session 23 – Pumped Storage, Role in the Grid; September 29, 2010; *International Journal on Hydropower & Dams,* Wallington, Surry, UK SM6 6AN, 2010.

6. Are Suul, Jon, "Variable Speed Pumped Storage Hydropower Plants for Integration of Wind Power in Isolated Power Systems," Norwegian University of Science and technology, 2009.

7. Gao, H.M., and C. Wang, "A Detailed Pumped Storage Station Model for Power System Analysis," 1-4244-0493-2/06 IEEE, 2006.

8. Kopf, E., S. Brausewetter, M. Giese, and F. Moser, "Optimized Control Strategies for Variable Speed Machines," 22nd IAHR Symposium on Hydraulic Machinery and Systems, June 29–July 2, Stockholm, 2004.

9. Grotenburg, K., F. Koch, I. Erlich, and U. Bachmann, "Modeling and Dynamic Simulation of Variable Speed Pump Storage Units Incorporated into the German Electric Power System," Graz, EPE, 2001.

10. Erlich, I., and U. Bachmann, “Dynamic Behavior of Variable Speed Pump Storage Units in the German Electric Power System,” 15th Triennial World Congress, Barcelona, Spain, 2002.

11. Liang, J., and R.G. Harley, “Pumped Storage Hydro-plant Models for System Transient and Long–term Dynamic Studies,” 978-1-4244-8357-0/10, IEEE, ???.

12. Kerkman, R.J., T.A. Lipo, W.G. Newman, and J.E. Thirkell, “An Inquiry into Adjustable Speed Operation of a Pumped Hydro Plant,” Parts 1 and 2, *IEEE Transactions on Power Apparatus and Systems*, Vol. PAS-99, No. 5, Sept./Oct., 1980.

13. Nagura, O., and M. Yoshida, “Transient Behavior Analysis of Adjustable Speed Pumped Storage System,” Hydro Vision International 2011, Session# 414; Sacramento, CA, July 20, 2011.

14. Akagi, H., “Large Scale Converters and Rectifier/inverter Based Systems,” *Proceedings of the IEEE*, Vol. 89, No. 6, June 2001.

15. Turel, V., F. Prime, and T. Machino, “Implementation of a Variable Speed Unit in the AVCE PSPP,” Hydro 2008 Conference, Ljubljana, Slovenia, October 6–8, 2008.

16. Donalek, P., H. Clark, R. Nakata, and J. Stein, “Application of Adjustable Speed Doubly Fed Machines in Pumped Storage and Conventional Hydroelectric Plants,” *Proceedings of the American Power Conference*, Chicago, IL, Vol. 55-I, pp. 245–290, April 1993.

17. Donalek P., and H. Clark, *Application of Adjustable Speed Machines in Conventional and Pumped Storage Hydro Projects*, EPRI, Palo Alto, CA 94304, November 1995.

18. Pannatier, Y., C. Nicolet, B. Kawkabani, J.-L. Deniau, A. Schwery, F. Avellan, and J.-J. Simond, “Transient Behavior of Variable Speed Pumped-Turbine Units,” 24th IAHR Symposium on Hydraulic Machinery and Systems, October 27–31, Foz Do Iguassu, 2008.

19. Hodder, A., “Double-fed Asynchronous Motor-generator Equipped with a 3-level VSI Cascade,” Ph.D. Thesis TH2939, École Polytechnique Federale de Lausanne (EPFL), 2004.

20. Kopf, E., S. Brausewetter, M. Giese, and F. Moser, “Optimized Control Strategies for Variable Speed Machines,” 22nd IAHR Symposium on Hydraulic Machinery and Systems, Stockholm, Sweden, June 29–July 2, 2004.

21. Nicolet, C., Y. Vaillant, B. Kawkabani, P. Allenbach, J.-J. Simond, and F. Avellan, “Pumped Storage Units to Stabilize Mixed Islanded Power Network—Transient Analysis,” Hydro 2008 Conference, Ljubljana, Slovenia, October 6–8, 2008.

Decision and Information Sciences
Argonne National Laboratory
9700 South Cass Avenue, Bldg. 221
Argonne, IL 60439-4844

www.anl.gov

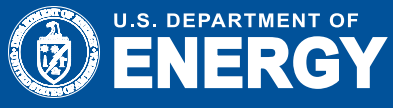

Argonne National Laboratory is a U.S. Department of Energy
laboratory managed by UChicago Argonne, LLC